CrossMark

TiO$_2$/polypyrrole nanocomposites photoactive under visible light synthesized by heterophase polymerization in the presence of different surfactants

**Blanca E. Castillo-Reyes · Víctor M. Ovando-Medina ·
Omar González-Ortega · Pedro A. Alonso-Dávila ·
Isaías Juárez-Ramírez · Hugo Martínez-Gutiérrez ·
A. Márquez-Herrera**

Abstract TiO$_2$/polypyrrole nanocomposites were synthesized by batch (B) and semi-batch (SB) heterophase polymerization of pyrrole onto TiO$_2$ nanoparticles. Sodium bis-2-ethylhexyl sulfosuccinate (AOT), hexadecyltrimethylammonium bromide (CTAB), and sodium dodecyl sulfate (SDS) were used as surfactants while ammonium persulfate served as oxidizing agent. The resulting nanocomposites were analyzed by scanning electron microscopy, Fourier transform infrared spectroscopy, X-ray diffraction, transmission electron microscopy, energy dispersive X-ray spectroscopy, UV/Vis diffuse reflectance spectroscopy, Raman spectroscopy, and cyclic voltammetry. TiO$_2$/polypyrrole nanoparticles were tested as photocatalysts

B. E. Castillo-Reyes · O. González-Ortega · P. A. Alonso-Dávila
Facultad de Ciencias Químicas, Universidad Autónoma de San Luis Potosí, Av. Dr. Manuel Nava No. 6, Zona Universitaria, 78240 San Luis Potosí, SLP, Mexico

V. M. Ovando-Medina (✉)
Ingeniería Química, Coordinación Académica Región Altiplano (COARA), Universidad Autónoma de San Luis Potosí, Carretera a Cedral KM 5+600, San José de las Trojes, 78700 Matehuala, San Luis Potosí, SLP, Mexico
e-mail: ovandomedina@yahoo.com.mx

I. Juárez-Ramírez
Departamento de Ecomateriales y Energía, Facultad de Ingeniería Civil, Universidad Autónoma de Nuevo León, Cd. Universitaria, 66450 San Nicolás de los Garza, Nuevo León, Mexico

H. Martínez-Gutiérrez
Centro de Nanociencias y Micro y Nanotecnologías, Instituto Politécnico Nacional (IPN), Luis Enrique Erro S/N, 07738 Mexico, D.F., Mexico

A. Márquez-Herrera
Departamento de Ingeniería Agrícola, DICIVA, Campus Irapuato-Salamanca, Universidad de Guanajuato, Ex Hacienda el Copal KM 9, Carretera Irapuato-Silao, 36500 Irapuato, Gto, Mexico

under visible light in the degradation of methylene blue. Nanocomposites with conductivities between 4.85×10^{-7} and 1.88×10^{-2} S/cm were obtained. It was concluded that the polymerization mode and the surfactant type, used as a stabilizing agent, have a strong effect on the photocatalytic activity of the materials. The best results were obtained when SDS was used and polymerization carried out in SB mode. Percentage of photodegradation under visible light after 15 min was as follows: TiO_2 1.7 %, CTAB-SB 25.5 %, SDS-B 39.6 %, CTAB-B 57.5 %, AOT-SB 69.4 %, AOT-B 80.1 %, and SDS-SB 94.1 %; while under UV light irradiation after 60 min the percentages were: SDS-B 64 %, CTAB-SB 67 %, CTAB-B 69 %, TiO_2 71 %, AOT-SB 88.2 %, AOT-B 95.0 %, and SDS-SB 96.5 %.

Keywords Heterophase polymerization · Polypyrrole · Nanocomposite · TiO_2 · Photocatalyst

Introduction

Composites of conducting polymer/inorganic materials have been considered as a new class of materials due to their improved properties compared with those of pure conducting polymers or inorganic materials. Inorganic nanoparticles can be introduced into the matrix of a host-conducting polymer either by some suitable chemical route or by an electrochemical incorporation technique [1]. Nanoparticles can be prepared by sol–gel [2], hydrothermal [3], emulsions, miniemulsions, and microemulsions methods [4–6]. However, microemulsion systems are more advantageous because it is possible to obtain polymeric nanoparticles with diameters smaller than 50 nm, polymers with high molar mass, and a variety of microstructures, which influence polymer properties [7]. Particularly, microemulsions are thermodynamically stable systems and formed spontaneously by mixing oil and water in the presence of an appropriate amount of a surfactant with a co-surfactant [8].

In the case of TiO_2/polypyrrole nanoparticles, improvements of the bulk properties such as electronic transference have been reported when compared with pure TiO_2, which can be used as a photocatalyst in the degradation of some organic compounds [9]. Polypyrrole (PPy) is easy to prepare by electrochemical techniques and its surface charge characteristics can easily be modified by changing the dopant anion (X^-) that is incorporated during the synthesis. The chemical polymerization of pyrrole is particularly important because this route is more practical for large-scale production of PPy with low cost. The effects of oxidant type and TiO_2 particle loading level on the physicochemical properties of the PPy/TiO_2 nanocomposites have been studied. For example, Deivanayaki et al. [10] synthesized PPy/TiO_2 nanoparticles using ammonium persulfate served (APS) as oxidizing agent changing the amount of TiO_2 (30, 40 and 50 wt%). They confirmed by Fourier transform infrared spectroscopy (FTIR) analysis the interaction between TiO_2 and PPy by the presence of small bands at 1,699 and 1,107 cm^{-1} corresponding to Ti–O–C. Wei et al. [11] studied the effects of the oxidant type (APS and $FeCl_3$) and the amount of TiO_2 on the physicochemical properties of PPy/TiO_2 nanocomposites, noting that

conductivity increased for the particles synthesized using $FeCl_3$ because the oxidation–reduction potential is lower compared with material synthesized with APS. On the other hand, Luo et al. [12] synthesized nanoparticles varying the ratio of PPy and TiO_2 under different conditions by in situ chemical oxidative polymerization and temperatures ranging from 0 to 45 °C using $FeCl_3$ as oxidant. The degradation of methyl orange in aqueous solution was carried out to evaluate the photocatalytic activity of the resulting material. It was found that PPy/TiO_2 nanocomposites showed significantly higher photocatalytic activities than pure TiO_2 under visible and UV light irradiation, while the highest photocatalytic activity of PPy/TiO_2 nanocomposites was obtained when the molar ratio of pyrrole monomer to TiO_2 was 1:100, the polymerization temperature was 0 °C, and the polymerization time was 4 h. Shi et al. [8] developed four different syntheses to generate polypyrrole nanoparticles with TiO_2 using $AgNO_3$ and $Fe(NO_3)_3$ under UV light irradiation and electrochemical methods to discover their effects on the morphology of nanoparticles and photodegradation of rhodamine B. They observed that the better performance in degradation of rhodamine B was achieved in the presence of material based on PPy nanoparticles with $AgNO_3$ and TiO_2. Other authors have synthesized nanowires based on PPy/TiO_2 by an electrospinning method using $FeCl_3$ as oxidizing agent in vapor phase polymerization to generate PPy [13].

New syntheses methods are based on the use of surfactants; however, to the best of our knowledge, no reports exist dealing with the effects of the surfactant nature and the polymerization mode of pyrrole on the photocatalytic properties of TiO_2/PPy materials. For example, Zhang et al. [14] synthesized PPy/TiO_2 microbelts by in situ polymerization of PPy onto TiO_2 as template using sodium dodecylbenzene sulfonate (SDBS) as surfactant and varying the ratio of PPy/TiO_2. The microbelts were tested on the degradation of methyl orange under UV light irradiation and they found that an enhanced photocatalytic activity can be achieved decreasing the PPy/TiO_2 relationship. This is obvious because TiO_2 photoactivity is maximized in the UV light wavelength range. Xiangzhong et al. [15] synthesized PPy/TiO_2 nanoparticles by polymerization in reverse phase microemulsion using CTAB as surfactant in hexanol. They observed spherical particles with diameters between 150 and 200 nm; however, composites tend to form clusters.

The objective of this work was the synthesis and characterization of TiO_2/PPy nanoparticles by heterophase polymerization of pyrrole in the presence of three different surfactants (SDS, CTAB and AOT), and with two polymerization modes: batch and semi-batch. The performance of the synthesized nanocomposites was also studied in the photodegration of methylene blue under visible light, which is not dangerous and has a lower cost than UV light.

Experimental

Materials

Pyrrole monomer (Py > 98 %), ammonium persulfate (APS > 98 %), surfactants sodium dodecyl sulfate (SDS > 98.5 %), hexadecyltrimethylammonium bromide

(CTAB > 98 %), and dioctyl sodium sulfosuccinate (AOT > 96 %) were acquired from Sigma-Aldrich and used as received. TiO_2 nanoparticles were purchased from Degussa (DP25). Methanol was acquired from Fermont (>99.9 %). Distilled grade water was used in all the experiments.

Polymerizations

Compositions used in polymerizations are shown in Table 1. In a typical synthesis, 39 g of water were mixed with surfactant in a 60-mL vial. Subsequently, 250 mg of TiO_2 were added and ultrasonicated (Cole-Parmer Instruments, CPX 130) for 10 min; then APS was added and homogenized in 1 mL of water with magnetic stirring. In batch polymerizations (B), 0.4 g of pyrrole was added in one shot. The reaction proceeded under magnetic stirring for 2 h. In semi-batch (SB) polymerization mode, pyrrole was loaded into a syringe fixed to an infusion pump (KdScientific) at a rate of 0.0133 g/min; the reaction mixture was allowed to react for 2 h after monomer addition. The reaction mixture was poured into an excess of methanol to precipitate the TiO_2/PPy nanoparticles. The samples were decanted and dried at 60 °C in an oven during 24 h. Conversions were determined gravimetrically by repeating the polymerizations, drying the total reaction mixture and subtracting the known weights of surfactant, APS, and TiO_2 from the total weight of dried samples. The final ratios of TiO_2/PPy in the purified composites were determined by thermogravimetric analysis (TA Instruments, Q600), 10 mg of each sample was heated between 25 and 800 °C at a heating rate of 10 °C/min.

Characterization

The resulting materials were analyzed using UV/Vis NIR diffuse reflectance spectroscopy measured between 300 and 800 nm using a spectrometer (Agilent, Cary 5000) equipped with an integrating sphere. The samples were also analyzed by FTIR spectroscopy (Agilent, Cary 630) and by Raman spectroscopy (B&W TEK). SEM analysis was completed (JEOL high resolution scanning electron microscope, JSM 7800F in STEM mode at 30 kV of beam acceleration) diluting latexes of TiO_2/PPy without purification 1:100 in distilled water. A drop of the diluted latex was poured onto a copper grid coated with Formvar[TM] resin and carbon film, and then

Table 1 Studied compositions of pyrrole (Py) polymerization

Run	Surfactant	TiO_2[a]	APS[a]	Py[a]
SDS-B	0.8 (SDS, batch)	0.25	1.36	0.4
SDS-SB	0.8 (SDS, semi-batch)	0.25	1.36	0.4
CTAB-B	0.8 (CTAB, batch)	0.25	1.36	0.4
CTAB-SB	0.8 (CTAB, semi-batch)	0.25	1.36	0.4
AOT-B	0.8 (AOT, batch)	0.25	1.36	0.4
AOT-SB	0.8 (AOT, semi-batch)	0.25	1.36	0.4

[a] All the amounts are in grams

allowed to dry overnight at room temperature. Elemental analysis was performed by energy dispersive X-ray spectroscopy (EDS) using a detector coupled to SEM. The X-ray diffraction (XRD) measurement was performed with a Phillips X'pert diffractometer using the CuKa line (kka1 = 1.54056 Å and kka2 = 1.54439 Å). Powders of pure TiO_2 were observed via transmission electron microscopy (TEM) using a JEOL-2010 system operated at 200 kV, and the powders were dispersed onto copper grids. The specific surface areas (A_{BET}) of composites were determined by N_2 physisorption (Micromeritics, ASAP 2020) using the Brunauer, Emmett, Teller (BET) method.

The electrical conductivities of samples were determined by the four-probe method (SP4 probe head Lucas/Signatone with 0.04 inches of spacing between tips) coupled to a Keithley (2400 SourceMeter) instrument. The cyclic voltammetry measurements were performed in a glass cell using a potentiostat/galvanostat GAMRY (G-300). Platinum disc, platinum wire, and Ag/AgCl electrodes were used as the working, counter, and reference electrodes, respectively. Voltammetry scans were carried out by dispersing 0.2 g of a sample in 100 mL of 0.1 M H_2SO_4 aqueous solution at room temperature in a potential range from +0.10 to +1.4 V using a scanning rate of 150 mV/s.

Photoactivity of synthesized materials

TiO_2 and TiO_2/PPy nanoparticles synthesized through different conditions were tested in methylene blue dye photodegradation in aqueous solutions. In order to compare with pure TiO_2, 175 mg of TiO_2/PPy nanoparticles were well dispersed in 50 mL of an aqueous solution of methylene blue dye at 20 mg/L under magnetic stirring in the dark through 30 min to achieve physical equilibrium adsorption. Solutions were exposed to a visible light source from a halogen lamp with tungsten filament (ADIR 1490, 500 W) at 40 cm from solutions to avoid heating or a UV light source consisting of a UV lamp of high intensity (UVP Black-Ray, 100 W and 365 nm wavelength, light intensity of 21 mW/cm^2 at 2 in.) at room temperature. To determine light intensity using the halogen lamp (visible light) over the surface of solutions, a light meter (CEM, DT1308) was used, giving a light intensity of 28.1 mW/cm^2. Samples of 0.5 mL were withdrawn at different times and centrifuged to determine UV/Vis spectra and absorbance (Genesys 10, Thermo-Spectronic) at a wavelength of 664 nm to calculate concentrations from a previous calibration curve.

Adsorption isotherm and kinetics determination

Batch adsorption experiments were performed at 25 °C as follows: 0.1 g of composite were added to a protected from light vial along with 30 mL of a methylene blue dye solution of known concentration in the range from 10 to 500 mg/L. Vials were continuously stirred using an orbital shaker (INO 650V-7) at constant temperature for 5 days. Adsorbed dye concentration at equilibrium (q) was calculated by a mass balance using the initial and final dye concentrations in solution. Concentrations of methylene blue throughout adsorption experiments were

determined in a spectrophotometer (Genesis 10S UV/Vis) using a calibration curve constructed with standard solutions at a wavelength of 664 nm. Adsorption kinetics experiments were run similar to batch adsorption (MB initial concentration set to 20 mg/L) but determining solution concentrations at different times until the equilibrium concentration was reached.

Results and discussion

Reaction mixtures were white and opaque before polymerization of pyrrole; they became dark at the beginning of polymerization and totally black at the end of polymerizations which is typical of PPy formation. The final compositions of PPy in the composites determined by TGA are shown in Table 2, in which it can be seen that these values are between 60.3 and 69.4 %, which are different to those estimated by gravimetry; this difference is due not only to TiO_2 nanoparticles loss during purification process but also to different pyrrole monomer conversions achieved in each synthesis. However, as will be discussed later, the photocatalytic performance of composites has a complex relationship with composite compositions, superficial area, and the surfactant type used in the composite preparation. Figure 1 shows the UV/Vis–NIR spectrum of pure TiO_2 and the corresponding spectra of TiO_2/PPy nanoparticles obtained in the different syntheses. Only one absorption band with a maximum at 300 nm is observed in Fig. 1 for pure TiO_2, which is characteristic of TiO_2 [16]. However, due to the presence of PPy, two absorption bands are present in TiO_2/PPy nanoparticles. It has been previously reported that, for pure PPy synthesized in similar conditions, two bands are usually perceived, one between 400 and 500 nm and a second band between 700 and 1,100 nm when SDS is used as surfactant [17]; however, when CTAB is used, the second band is less noticeable [18]. In the present work, the first band is observed between 200 and 350 nm, with a maximum around 300 nm, and the second band between 360 and 700 nm.

The first band has been attributed to transitions of the valence band to the polaron state [19], and is directly related to the conductivity of the PPy chain (high degree of π conjugation, i.e. π–π* interactions along the polymer chain). The second band is

Table 2 Compositions of PPy (%) in the different materials calculated from pyrrole conversions by gravimetry and from TGA analysis, and the BET area

Run	Gravimetry	TGA	BET area (m^2/g)
Pure TiO_2	0	0	–
SDS-B	58.4	69.4	25
SDS-SB	46.5	68.1	56
CTAB-B	57.8	63.6	27
CTAB-SB	56.3	60.3	22
AOT-B	58.3	66.0	46
AOT-SB	47.5	68.4	39
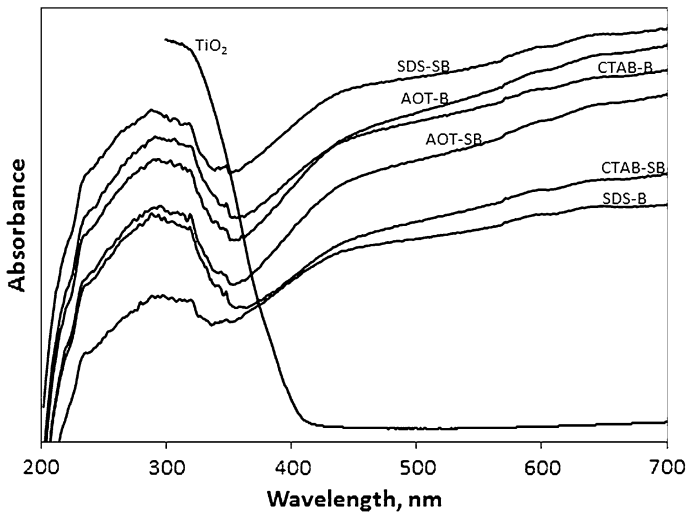
Fig. 1 UV/Vis–NIR spectra from pure TiO_2 nanoparticles and TiO_2/PPy nanocomposites obtained under different conditions

related to the bipolaron state of PPy. Usually, the bipolaron state is observed when some dopant agent is present in the conducting polymer chain. The reason for the absorption bands being shifted to lower wavelengths can be ascribed to a strong interaction of PPy chains with the TiO_2. However, UV/Vis–NIR spectra indicate that TiO_2/PPy materials could also be active in the visible light region. Therefore, it is expected that all prepared compounds can be used as active materials for the methylene blue degradation not only under UV light but also under visible light irradiation.

Figure 2 shows the FTIR spectra of materials from different syntheses, including the corresponding to pure TiO_2 nanoparticles. In Fig. 2c, the characteristic signals of TiO_2 cannot be observed because Ti–O–Ti vibration usually appears as a broad intense band around 660 cm^{-1}. Signals at 1,650 cm^{-1} and the strong band between 3,100 and 3,500 cm^{-1} have been ascribed to the absorption of hydrogen-bonded surface species (hydroxyl and water). The first band corresponds to the H–O–H bending vibration whereas the other one is assigned to the O–H stretching vibration [20]. In Fig. 2a, b, the characteristic peaks of PPy chains can be detected. The peak at 1,450 cm^{-1} is ascribed to the C–C ring stretching, the peak around 1,540 cm^{-1} is due to C=C backbone stretching, and the peaks at 1,310 and 1,180 cm^{-1} are due to the C–H in-plane and C–N stretching vibrations, respectively [21]. In the case in which CTAB was used, the signal at 1,540 cm^{-1} is negligible while the peak at 1,580 cm^{-1} cannot be ascribed to C=C. As reported by Deivanayaki et al. [10], peaks at 1,700 and 1,110 cm^{-1} correspond to Ti–O–C interactions. The integrated ratio intensities of C=C/C–C from infrared spectra is related to the conductivity of PPy chains because of longer effective π-conjugation along the PPy chains [22]. Conductivity values and
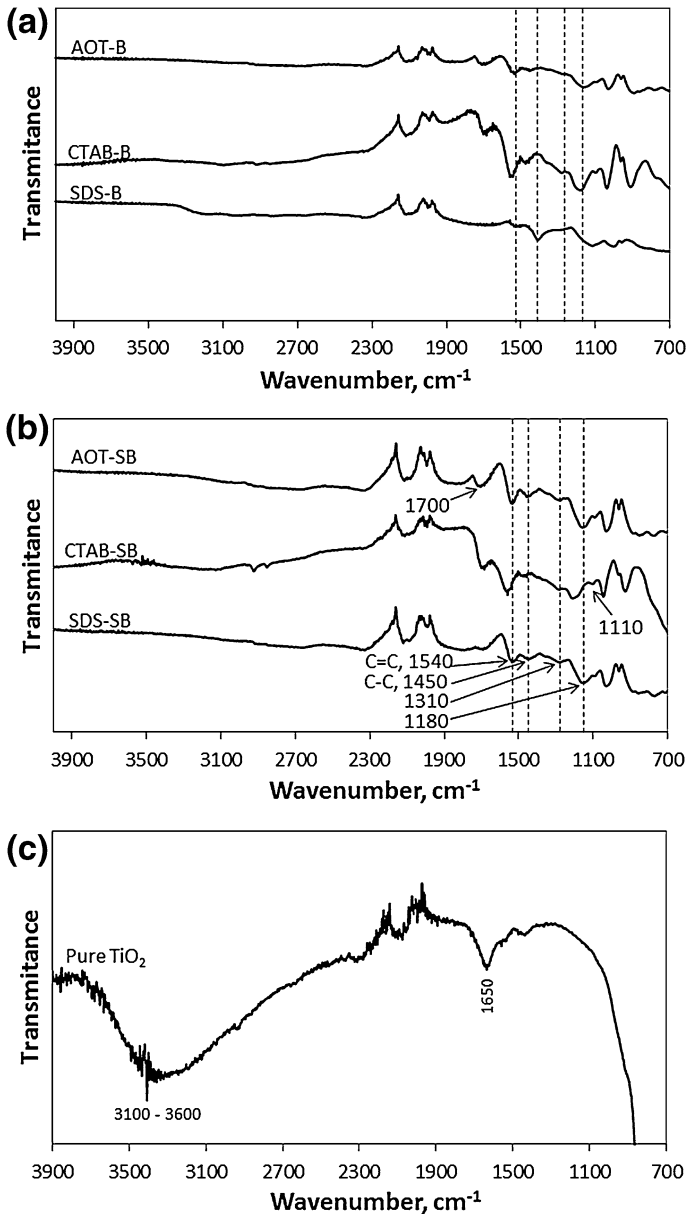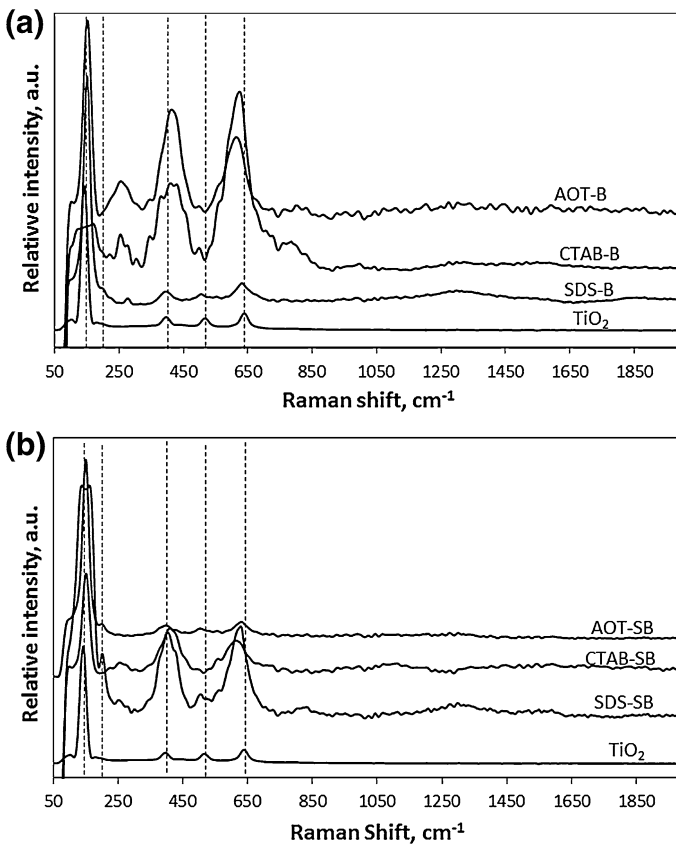
Fig. 2 FTIR spectra of TiO$_2$/PPy nanoparticles obtained with different surfactants in batch (**a**), semi-batch (**b**), and pure TiO$_2$ (**c**)

integrated ratio intensities of C=C/C–C from FTIR ($I_{C=C}/I_{C-C}$) are shown in Table 3, from which it can be observed that conductivities were in the order: (surfactant used-polymerization mode) SDS-B > SDS-SB > AOT-SB > CTAB-B > AOT-B > CTAB-SB, while the $I_{C=C}/I_{C-C}$ order was: AOT-B > AOT-SB > SDS-SB > SDS-B (CTAB

Table 3 Voltage of cathodic and anodic peaks from cyclic voltammetry, conductivities (C) of materials, and integrated ratio of C = C/C–C from FTIR analysis

Sample	Cathodic (V)	Anodic (V)	C (S/cm)	$I_{C=C}/I_{C-C}^a$
TiO$_2$	0.33	0.55	–	–
SDS-B	1.06	0.46	1.88×10^{-2}	0.204
SDS-SB	1.00	0.46	5.24×10^{-3}	2.869
CTAB-B	1.10	1.02	4.40×10^{-5}	–
CTAB-SB	1.06	0.92	4.85×10^{-7}	–
AOT-B	1.08	0.42	3.84×10^{-5}	3.744
AOT-SB	1.04	0.44	4.46×10^{-5}	3.160

[a] Integrated ratio of signals of C=C/C–C from FTIR analysis

Fig. 3 Raman spectra from pure TiO$_2$ and TiO$_2$/PPy nanoparticles obtained with different surfactants in batch (**a**) and semi-batch (**b**) polymerizations

signals were not integrated). Differences between conductivities and FTIR analyses can be derived from the presence of some surfactant molecules interacting with PPy chains, thus affecting the integrated areas.

The signals of TiO_2 can be clearly identified in the Raman spectra shown in Fig. 3. According to Ohsaka [23], six active Raman modes are allowed for anatase TiO_2 which must appear at 144 cm^{-1} (E_g), 197 cm^{-1} (E_g), 399 cm^{-1} (B_{1g}), 513 cm^{-1} (A_{1g}), 519 cm^{-1} (B_{1g}), and 639 cm^{-1} (E_g). In the present work, only five peaks can be observed at 630, 500, 380, 180, and 140 cm^{-1} for pure TiO_2. However for the TiO_2/PPy nanoparticles, depending on surfactant type and polymerization mode, these signals are displaced to lower values with enhanced intensities. Moreover some new signals are observed near to 200, 250, and 550 cm^{-1}. These can be ascribed to strong interactions of TiO_2 with PPy and surfactant molecules.

Figure 4 shows the X-ray diffractograms of the samples obtained in the different syntheses, while the positions of diffraction peaks associated to the tetragonal TiO_2 from the 211,276 and 211,272 cards of the Powder Diffraction File database are also shown. It can be seen that the peaks presented in the experimental diffractograms are due to the diffraction of the anatase phase, while some rutile phase can also be observed. Absence of signals corresponding to PPy implies that most likely only the amorphous form of polymer was obtained in all syntheses.

The voltammetry curves of synthesized materials are shown in Fig. 5. Here, the characteristic redox behavior of PPy is clearly seen [19], with an oxidation peak (cathodic) around +1.0 V while the reduction peak (anodic) is near to +0.4 V versus Ag/AgCl for samples obtained with SDS and AOT. The anodic peak for samples with CTAB showed lower redox activity. The cathodic and anodic peaks are shown in Table 3, from which it can be seen that pure TiO_2 shows negligible
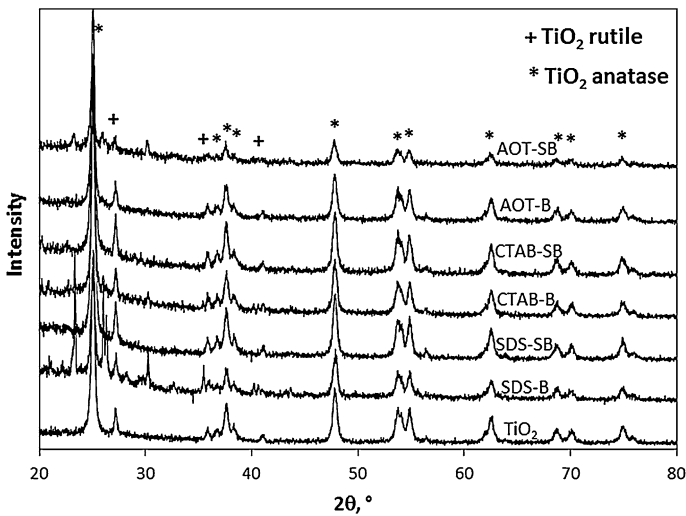
Fig. 4 XRD spectra from pure TiO_2 and TiO_2/PPy nanoparticles obtained with different surfactants in batch and semi-batch polymerizations
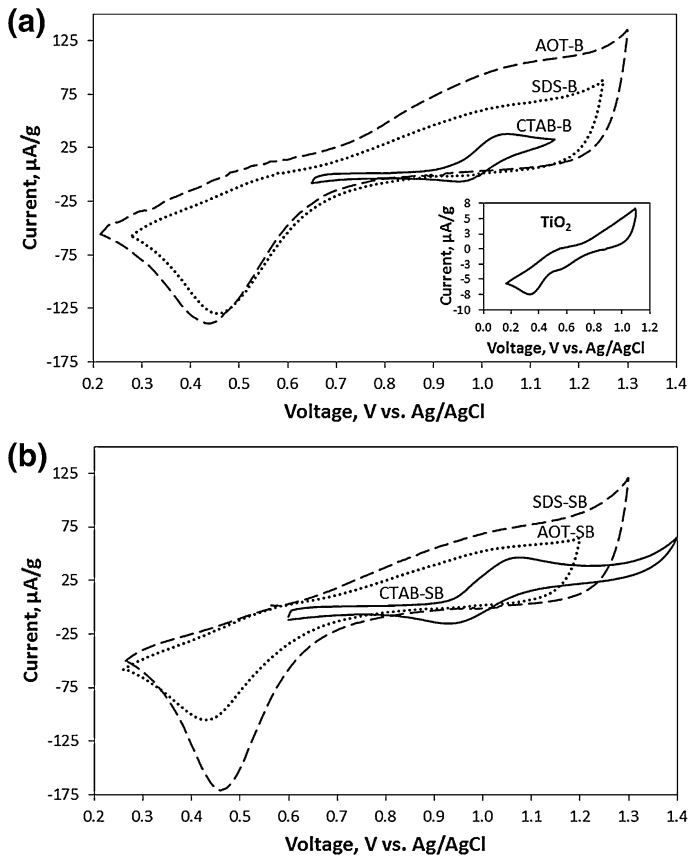
Fig. 5 Cyclic voltammetry of samples obtained under different conditions: **a** batch, and **b** semi-batch

redox activity compared to samples with PPy (inset in Fig. 5a). The sample with the best redox activity was that synthesized with SDS in SB mode. Redox activity increased from batch to semi-batch polymerization mode when CTAB and SDS were used, while it decreased when using AOT.

Figure 6 shows the transmission electron micrograph of pure TiO_2 nanoparticles and its particle size distribution (PSD). The number- and weight-average particle diameters (D_n and D_w, respectively) and polydispersity index (PDI) of TiO_2 nanoparticles were calculated counting at least 300 particles from various scanning electron micrographs using ImageJ 1.37c software with the following equations [17]:

$$D_n = \sum n_i D_i / n_i \tag{1}$$

$$D_w = \sum n_i D_i^4 \Big/ \sum n_i D_i^3 \tag{2}$$

$$PDI = D_w / D_n \tag{3}$$

where n_i is the number of particles with diameter D_i.
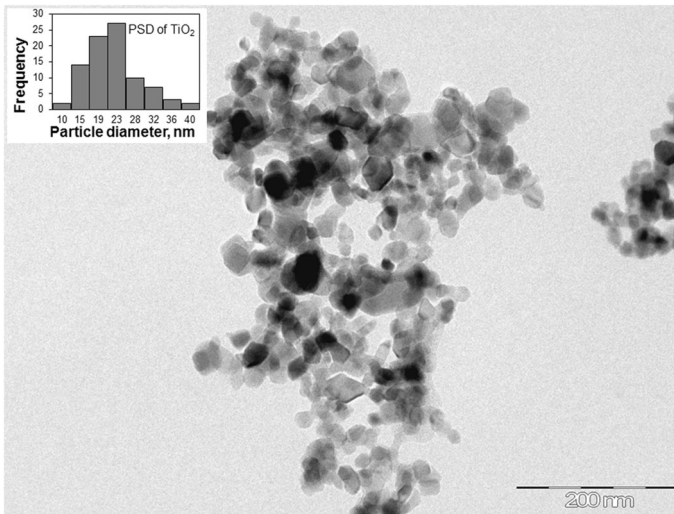
Fig. 6 Transmission electron micrograph (TEM) of pure TiO_2 nanoparticles

It can be seen from Fig. 6 that almost spherical nanoparticles of TiO_2 are present with diameters between 10 and 40 nm. Number-average diameter was calculated as 24 nm with PDI of 1.2, showing narrow PSD. Furthermore, no agglomeration was observed. Figure 7 shows SEM images of TiO_2/PPy nanoparticles from samples AOT-B and SDS-SB. TiO_2 nanoparticles are well coated with semiconducting PPy; however, more agglomeration is observed for AOT-B than for SDS-SB and thus SDS surfactant gives higher particle stabilization through pyrrole polymerization. In order to differentiate the PPy from TiO_2 phases of composite, a sample of SDS-SB was studied by EDS. Figure 8 shows an SEM image in STEM mode of this sample. The circle and triangle indicate where EDS were made. It can be seen in Figs. 9 (corresponding to the circular area in Fig. 8) and 10 (corresponding to the triangular area in Fig. 8) that in the circular area a high amount of Ti and oxygen are present with a small amount of carbon, while in the triangular area of Fig. 8 a high amount of carbon with a very small amount of Ti and no oxygen was detected. These results imply that TiO_2 nanoparticles were totally immersed in a PPy matrix.

Figure 11 shows the UV/Vis spectra of methylene blue solutions during photodegradation in the presence of the different synthesized materials and in the presence of pure TiO_2 nanoparticles, under visible light after 1 min of reaction and under UV light after 15 min of reaction. Under visible light irradiation, CTAB-SB samples showed very low photocatalytic activity when compared to pure TiO_2; however, TiO_2, CTAB-SB, and SDS-B samples showed poor photocatalytic performance under visible light when compared to the other test samples. Better performance can be observed for the same conditions using CTAB-B, AOT-SB, AOT-B, and SDS-SB. Signals of methylene blue using SDS-SB practically disappeared after 1 min of reaction. On the other hand, under UV light irradiation, photodegradation rates were slower (15 min were needed to observe considerable
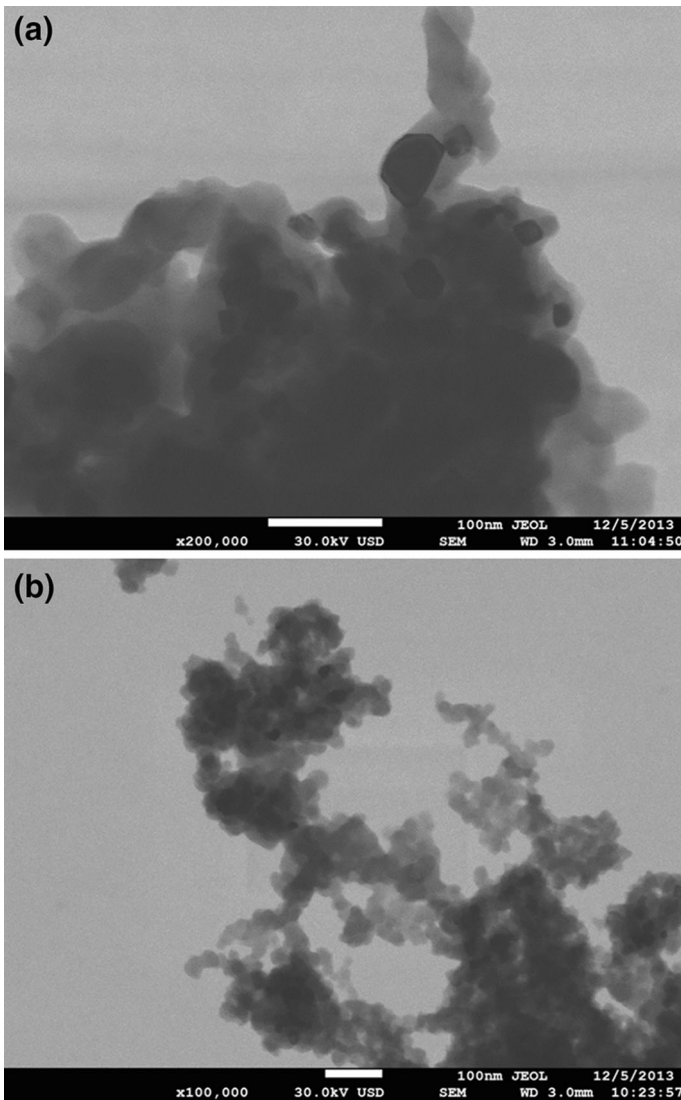
Fig. 7 Representative scanning electron micrograph (SEM) of AOT-B (**a**) and SDS-SB (**b**) samples

changes) resulting in a better photocatalytic behavior for the samples AOT-SB, SDS-SB, and AOT-B. The ratios of concentrations at a given time/initial concentration (C/C_0) of methylene blue through photodegration using the synthesized materials and TiO_2 nanoparticles are shown in Fig. 12. It can be observed for all composites that C/C_0 decreased drastically in the first 3 min for visible light irradiation, and in the first 15 min under UV light irradiation, and then continued decreasing at a lower rate. Percentages of photodegradation under visible light after 15 min were as follows: TiO_2 1.7 %, CTAB-SB 25.5 %, SDS-B 39.6 %, CTAB-B
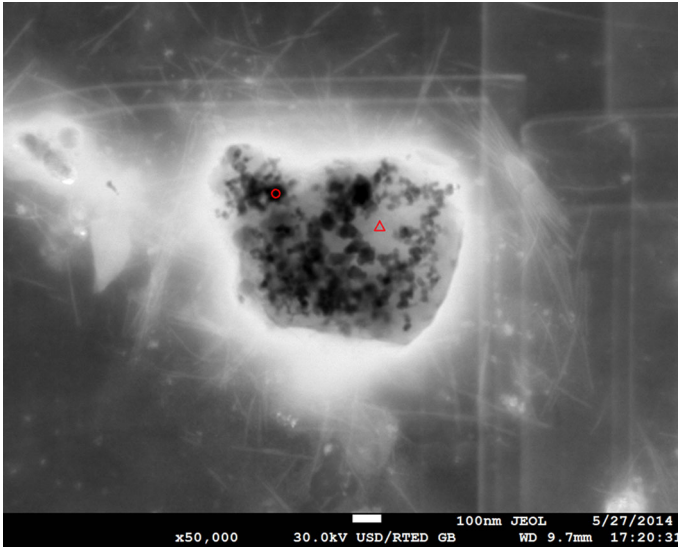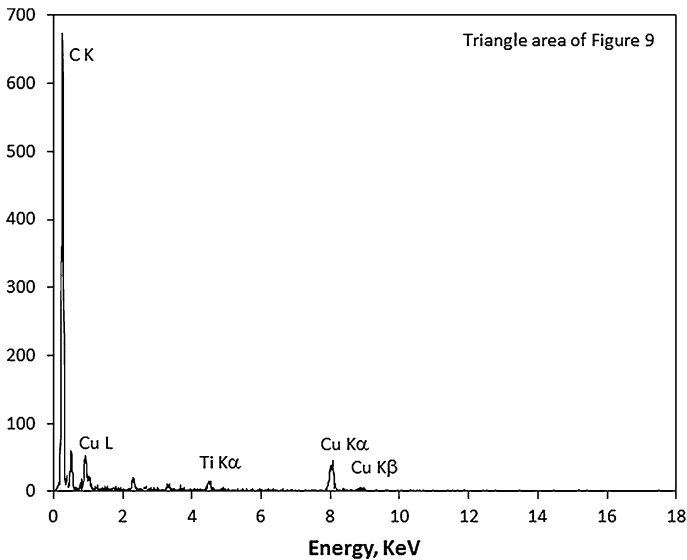
Fig. 8 SEM image in STEM mode of sample SDS-SB
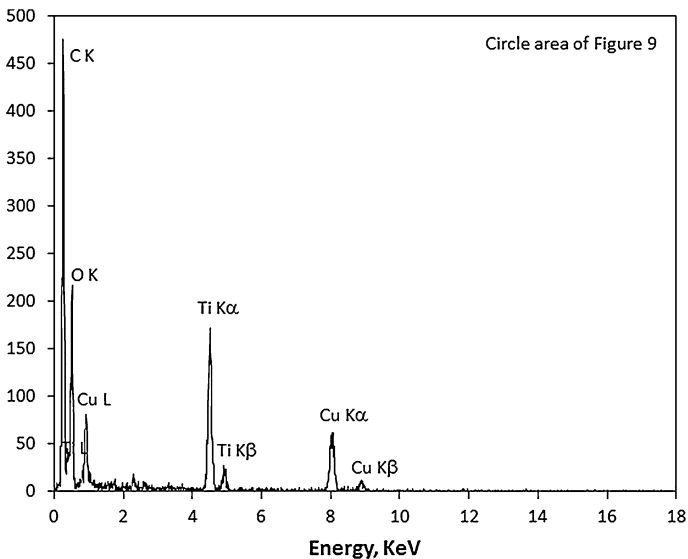
Fig. 9 EDS spectrum of sample SDS-SB corresponding to circular area of Fig. 8

57.5 %, AOT-SB 69.4 %, AOT-B 80.1 %, and SDS-SB 94.1 %; while under UV light irradiation after 60 min, the corresponding percentages were: SDS-B 64 %, CTAB-SB 67 %, CTAB-B 69 %, TiO_2 71 %, AOT-SB 88.2 %, AOT-B 95 %, and SDS-SB 96.5 %. Although the samples were washed several times with methanol,

Fig. 10 EDS spectrum of sample SDS-SB corresponding to triangular area of Fig. 8

some surfactant molecules remained strongly attached to TiO_2/PPy materials. It is clear that better results were observed with the anionic (SDS and AOT) than with the cationic surfactant (CTAB). This behavior can be ascribed to electrostatic interactions between methylene blue, which is a cationic dye, and the surfactant molecules. When using CTAB as surfactant, methylene blue molecules are repelled thus diminishing the photodegradation rate. However, when an anionic dye such as reactive red 120 was used instead of methylene blue, better photodegradations were observed for materials synthesized in the presence of CTAB (data not shown). On the other hand, Table 2 shows the specific BET area of each composite, and it can be seen that the greater the specific area, the higher the photodegradation efficiency, in fact, a linear relationship between these two variables was observed.

TiO_2/PPy materials showed photoactivity in the visible light region, giving as a result the enhancement on the photodegration performance of the methylene blue, whereas pure TiO_2 is photoactive only under UV light irradiation. Oliveira and Oliveira [9] reported the synthesis of TiO_2/PPy nanoparticles, using AOT as stabilizing agent and $FeCl_3$ as the oxidizing agent, and tested the material in the photodegradation of rhodamine-B. We also synthesized TiO_2/PPy material as reported by Oliveira, and it was tested in the photodegradation of methylene blue under similar conditions used in our work. We observed that, after 15 min of photodegradation under visible light, 64.5 % of methylene blue degradation was achieved, while 94.4 % was observed under UV light irradiation.

Dimitrijevic et al. [24] reported the thermal polymerization (80 °C) of pyrrole onto TiO_2 nanoparticles to be used in the photodegradation of a diluted (15 μM or 4.8 mg/L) methylene blue solution. They found that the rate of MB degradation depended linearly on the concentration of TiO_2/PPy nanocomposites. Conductive
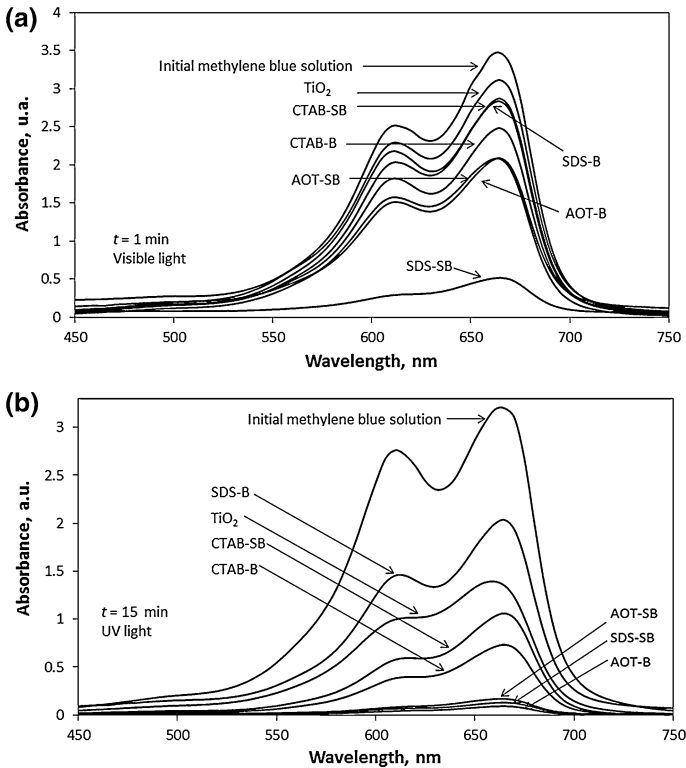
Fig. 11 UV/Vis spectra of methylene blue photodegradation under visible light after 1 min of reaction (**a**) and under UV light irradiation after 15 min of reaction (**b**)

polymers with extending π-conjugated electron systems, such as PPy, act as stable photosensitizers injecting electrons into the conduction band of TiO_2 and across the nanocomposite interface. Besides their high absorption coefficients in the visible part of the spectrum, conjugated polymers exhibit high mobility of charge carriers and excellent stability [24]. As mentioned in the "Introduction", the synthesis of TiO_2/PPy composites has been previously reported; however, we have demonstrated that not only the presence of conducting polymer is important to increase the photocatalytic activity of this composite but also the internal structure of the polymer, since, through PPy chain formation, linear and branched structures can be obtained [17], which can be affected by the polymerization mode and by the type of surfactant used as stabilizer.

In order to confirm that the decrease in MB concentration from solutions was by photodegradation instead of adsorption, experiments of adsorption were made to determine the kinetics and adsorption isotherm. Figure 13 shows the adsorption isotherm and kinetics (inset) from which it can be observed that only 10 % of MB was adsorbed after 1 min by the sample SDS-SB. After 30 min, equilibrium was reached and approximately 23 % of MB was removed
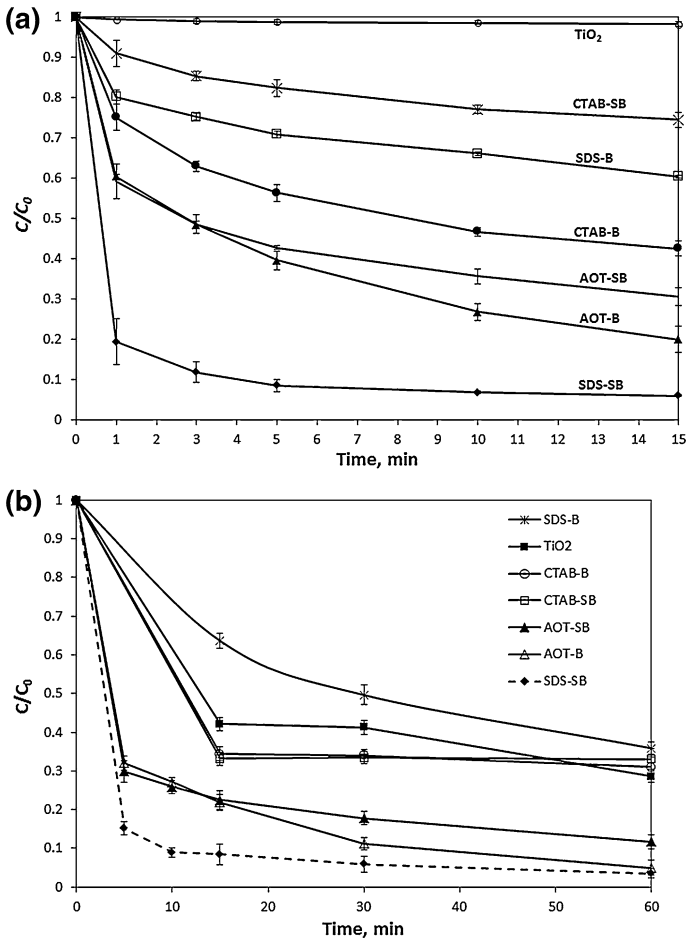
Fig. 12 Kinetics of methylene blue photodegradation under visible light (**a**) and UV light (**b**) irradiation at different reaction times

by adsorption. Thus, under visible light irradiation, MB was affectively photodegraded after 1 min. The adsorption process of a solute onto an adsorbent can be described by many adsorption isotherm models. The equilibrium adsorption isotherms are of fundamental importance in the design of any adsorption system. In this work, the experimental data of adsorption were well represented by the Langmuir model:

$$q = \frac{q_m K_L C_e}{1 + K_L C_e} \tag{4}$$

where q is the adsorption capacity at the equilibrium concentration (C_e), K_L is a Langmuir constant (related to the affinity of binding sites), and q_m is the maximum
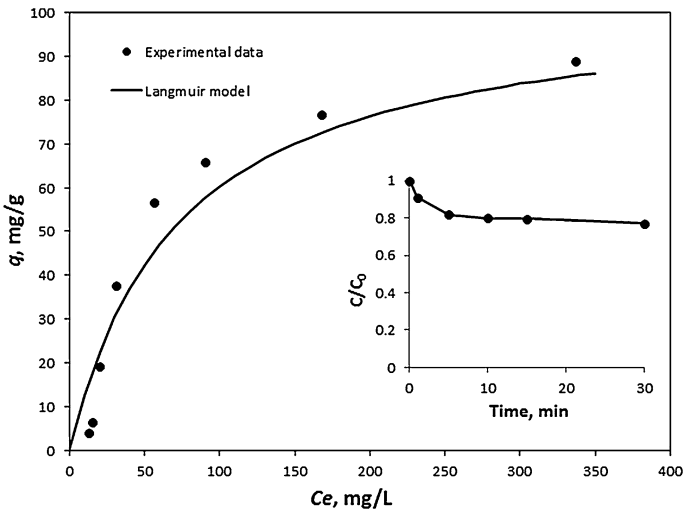
Fig. 13 Adsorption isotherm and kinetics of MB onto TiO2/PPy nanocomposite corresponding to sample SDS-SB

adsorption capacity. The Langmuir model assumes that the solid surface has a finite number of identical sites (homogeneous monolayer adsorption). The adjusted parameters were $q_m = 104.2$ mg/g and $K_L = 0.0137$ L/mg.

The characteristics of the Langmuir isotherm can be expressed in terms of a dimensionless equilibrium parameter (R_L), defined by $R_L = 1/(1 + K_L C_0)$, where C_0 is the initial concentration [25]. R_L indicated the shape of the adsorption isotherm: $R_L > 1$ is unfavorable adsorption, $R_L = 1$ is linear adsorption, $0 < R_L < 1$ is favorable adsorption and $R_L = 0$ is irreversible adsorption. Figure 14 shows the calculated R_L values as a function of C_0. It can be observed that adsorption is favorable at higher concentrations. Also, the value of R_L in the range from 0 to 1 at all initial dye concentrations which confirms the favorable uptake process of the methylene blue dye under the studied conditions.

The mechanism of dye photodegradation using the TiO_2/PPy composite is explained as follows: when visible light collides with the composite; the electrons are promoted from the highest occupied molecular orbital (HOMO) to the lowest unoccupied molecular orbital (LUMO) of the semiconducting PPy, and these electrons are injected to the conduction band (CB) of TiO_2, while holes will be left in the HOMO of PPy. The electrons in the valence band (VB) of TiO_2 move to the HOMO of PPy to recombine with these holes and, at the same time, holes generate in the VB of TiO_2. The photogenerated electrons are so active that they react with O_2 dissolved in water to generate superoxide $^{\cdot}O_2^{-}$, while holes can react with OH^{-} or water to generate $^{\cdot}OH$. These energetic species known as reactive oxygen species (ROS) can further react to form singlet oxygen $^{1}O_2$ [26, 27]. Therefore, the TiO_2 surface does not need to be directly in contact with MB dye molecules to photodegrade them under visible light.
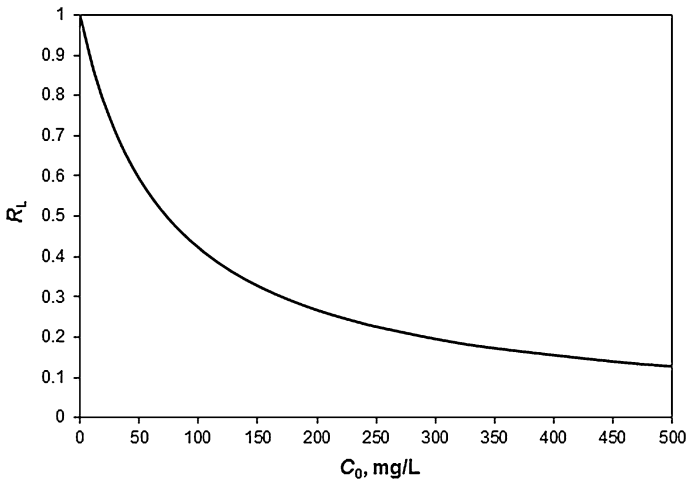
Fig. 14 Calculated dimensionless equilibrium parameter (R_L) from the K_L value obtained from the Langmuir model

From the obtained results, the PPy content in the final composites does not strongly affect the efficiency of photodegradation. However, it was observed that the A_{BET} has a very important effect when comparing each surfactant with respect to the polymerization mode; i.e., for the cationic surfactant, an increase of 5 m^2/g in the A_{BET}, which increased to twice the efficiency of photodegradation. On the other hand, for the anionic surfactant AOT, which has two hydrocarbon tails in its structure, it was observed that an increase of 7 m^2/g in the A_{BET} increased the efficiency photodegradation from 69.4 to 80.1 %, which are much higher values than those observed for the cationic surfactant CTAB, which changed from 25 to 57.5 %. For the anionic surfactant SDS, which has only one hydrocarbon tail, an increase in the A_{BET}, from 25 to 56 m^2/g, increased the efficiency of photodegradation from 39.6 to 94.1 %, respectively.

Due to the electric nature of surfactant attached to composites after purification, it would be expected that, for SDS and AOT surfactants (independently of polymerization mode), higher efficiencies of photodegradation would be observed than using CTAB, due to the better electric affinity between the surfactant and MB dye. Nevertheless, this behavior in the efficiency was different to that expected, then we conclude that the A_{BET} determines the efficiency. The higher A_{BET} observed polymerizing in SB mode using SDS might be due to better distribution of TiO$_2$ nanoparticles in the PPy matrix because a low monomer addition rate to reactor implies very low monomer accumulation, and thus PPy particles agglomeration are inhibited, increasing the A_{BET}. This behavior was not observed when polymerizing in batch mode for this particular surfactant. Due to the complex interaction of the polymerization mode with the surfactant nature, it is difficult to explain the correlations with the final A_{BET} under the studied conditions, and more work is needed.

Conclusions

Nanoparticles of TiO_2/PPy were successfully synthesized in the presence of different surfactants by batch and semi-batch polymerization processes. The as-synthesized nanoparticles showed photoactivity under visible light. The surfactant type and polymerization mode strongly affected the nanoparticles morphology, polymer conductivity, and the specific surface area, which impacted the photocatalytic performance of composites. It was observed that the best photocatalytic activity in methylene blue degradation was that using TiO_2/PPy nanoparticles synthesized in the presence of SDS as surfactant, while in SB polymerization mode, only 1 min of photodegradation was needed to achieve more than 80 % of photodegradation when compared to TiO_2 (Degussa P25). The latter achieved only 1.7 % of photodegradation under visible light irradiation, which was explained as a function of the specific surface area. Synthesized materials could be used in the photodegradation of some other organic dyes such as reactive red 120 under visible light irradiation, which is cheaper than UV light and not dangerous.

References

1. R. Gangopadhyay, A. De, Chem. Mater. **12**, 608 (2000)
2. S.T. Navale, G.D. Khuspe, M.A. Chougule, V.D. Patil, J. Phys. Chem. Solids **75**, 236 (2014)
3. K. Suresh Babu, V. Narayanan, Chem. Sci. Trans. **2**(S1), S33 (2013)
4. S.W. Zhang, S.X. Zhou, Y.M. Weng, L.M. Wu, Langmuir **21**, 2124 (2005)
5. J. Faucheu, C. Gauthier, L. Chazeau, J. Cavaille, V. Mellon, E. Bourgeat-Lami, Polymer **51**, 6 (2010)
6. F. Pavel, J. Disper, Sci. Technol. **25**, 1 (2004)
7. J.R. Herrera, R.D. Peralta, R.G. López, L.C. Cesteros, E. Mendizábal, J.E. Puig, Polymer **44**, 1795 (2003)
8. Y. Shi, Y. Wu, J. Hao, G.J. Li, Polym. Sci. Part A Polym. Chem. **43**, 203 (2005)
9. A. Oliveira, H. Oliveira, Polym. Bull. **70**, 579 (2013)
10. S. Deivanayaki, V. Ponnuswamy, R. Mariappan, P. Jayamurugan, Optik **124**, 1089 (2013)
11. S. Wei, P. Mavinakuli, Q. Wang, D. Chen, R. Asapu, Y. Mao, N. Haldolaarachchige, D. Young, Z. Guo, J. Electrochem. Soc. **158**, K205 (2011)
12. Q. Luo, X. Li, D. Wang, Y. Wang, J. An, J. Mater. Sci. **46**, 1646 (2011)
13. X. Lu, Q. Zhao, X. Liu, D. Wang, W. Zhang, C. Wang, Y. Wei, Macromol. Rapid Commun. **27**, 430 (2006)
14. C. Zhang, Q. Li, J. Li, Synth. Metals **160**, 1699 (2010)
15. R. Xiangzhong, L. Xi, L. Jianhong, L. Xun, Z. Peixin, Z. Qianling, L. Zhongkuan, L. Yi, Rare Metal Mater. Eng. **37**, 288 (2008)
16. R. Vijayalakshmi, V. Rajendran, Arch. Appl. Sci. Res. **4**, 1183 (2012)
17. V.M. Ovando-Medina, R.D. Peralta, E. Mendizábal, H. Martínez-Gutiérrez, T. Lara-Ceniceros, R. Ledezma-Rodríguez, Colloid Polym. Sci. **289**, 759 (2011)
18. V.M. Ovando-Medina, H. Martínez-Gutiérrez, M.A. Corona-Rivera, E. Cervantes-González, J. Flores-Mejía, L. Farías-Cepeda, Colloid Polym. Sci. **291**, 2131 (2013)
19. P. Saville, Pyrrole formation and use. Defence Research and Development Canada—Atlantic. Technical Memorandum 2005–2004, Canada
20. M.C. Rosu, R.C. Siciu, S.V. Dreve, T.D. Silipas, I. Bratu, E. Indrea, Rev. Roum. Chim. **56**, 601 (2011)
21. Y. Liu, Y. Chu, L. Yang, Mater. Chem. Phys. **98**, 304 (2006)
22. J. Choi, H. Kim, S. Haam, S.Y. Lee, J. Disp. Sci. Tech. **31**, 743 (2010)

23. T. Ohsaka, J. Phys. Soc. Jpn. **48**, 1661 (1980)
24. N.M. Dimitrijevic, S. Tepavcevic, Y. Liu, T. Rajh, S.C. Silver, D.M. Tiede, J. Phys. Chem. C **117**, 15540 (2013)
25. T.W. Weber, R.K. Chakkravorti, AIChE J. **20**, 228 (1974)
26. D. Wang, Y. Wang, X. Li, Q. Luo, J. An, J. Yue, Catal. Commun. **9**, 1162 (2008)
27. Y. Liao, J. Brame, W. Que, Z. Xiu, H. Xie, Q. Li, M. Fabian, P.J. Alvarez, J. Hazard. Mat. **260**, 434 (2013)